Appl. Phys. B 67, 689–697 (1998)

Applied Physics B
Lasers
and Optics

Decoding the dynamics of a single trapped atom from photon correlations

V. Gomer, B. Ueberholz, S. Knappe, F. Strauch, D. Frese, D. Meschede

Institut für Angewandte Physik, Universität Bonn, Wegelerstr. 8, D-53115 Bonn, Germany
(Fax: +49-228/733474, E-mail: gomer@iap.uni-bonn.de)

Received: 4 September 1998

Abstract. Information on the dynamics of a single neutral atom can be decoded from fluctuations in the resonance fluorescence. We have measured two-time photon correlations of individual cesium atoms stored in a magneto-optical trap. We observe strong correlations at nanosecond scales (Rabi oscillations), at microseconds (intensity and polarization correlations), and also at milliseconds (position correlations) revealing the dynamical behavior of the atomic excitation, of the atomic orientation, and of its transport in the trap at both the optical wavelength scale and the trap size. In this article we compare our experimental results with a simplified model of an atom moving through an optical lattice. We investigate the influence of light-field topography and of the multilevel character of the atom on the shape and the visibility of the correlations.

PACS: 32.80.Pj; 42.50.Vk; 42.50.Ar

Single microscopic particles such as atoms, ions, or molecules are very often at the heart of the theoretical descriptions of matter. Over the past decades it has become possible and is still a field of growing interest to directly perform experiments with individual particles. Trapping of individual atoms has been accomplished a long time ago for ions [1] but only recently for neutral atoms [2–4]. The observation of individual atoms eliminates ensemble properties, yielding new and complementary information about their dynamics. We have observed single atoms trapped for several minutes in a magneto-optical trap. Photon correlations measured in single atom fluorescence show high contrast and allow us to study atomic dynamics with good statistics and in a non-invasive manner.

In our experiments we observe excellent quality data with a gross structure which can be qualitatively understood in terms of simple atoms diffusing in a magneto-optical trap. A detailed theoretical understanding is complicated by both the complex structure of the light field and the multilevel structure of the real cesium atom used in our experiment. It is the purpose of this article to present our experimental data and compare them with a very simple theoretical model. For this purpose we begin by theoretically investigating the motion of a scalar atom in potential-free 1D standing-wave light fields and its influence on the resonance fluorescence. We will extend several aspects of this model with respect to dimensions, multilevel atomic structure, and periodic potential as a first step to a more thorough understanding of resonance fluorescence fluctuations.

1 Experimental

Trapping of few atoms in a magneto-optical trap (MOT) [5] for a long period of time is achieved by drastically reducing the trap capture rate from the low-pressure background vapor under good vacuum conditions.

We use a vapor cell MOT in the standard σ^+-σ^- polarization configuration with three orthogonal pairs of counterpropagating laser beams. All lasers are diode lasers whose output frequencies are controlled by optical and electronic feedback and which have short-term linewidth and long-term stabilities of well under 1 MHz. The cooling laser detuning is precisely controlled by heterodyne phase-locking to a diode laser. The latter has a linewidth of a few kHz and is stabilized to the center of the cesium cooling transition $F = 4 \rightarrow F' = 5$. The stability and reliability of the diode lasers allow to record the correlation measurements at constant experimental conditions for many hours, or even for days.

The MOT quadrupole magnetic field is produced by NdFeB permanent magnetic discs and is tunable up to 800 G/cm [4]. In measurements reported here we usually choose a magnetic filed gradient of 375 G/cm. In an earlier experiment [6], we have demonstrated that the the main influence of a steep gradient is a significant reduction of the capture rate [7], while the temperature of trapped atoms is comparable to a low-field MOT and therefore leads to a stronger localization. The measured spatial distribution of the MOT fluorescence has a Gaussian-like form with a 1/e

diameter of about 20 μm which is independent of the number N of stored atoms (for $N < 10$).

A strong reduction of the capture rate is essential for experiments with few atoms since the average atom number is given by the product of the capture rate and the mean time between collisions of trapped atoms with the residual gas molecules that kick an atom out of the trap. In our stainless steel chamber a base pressure of better than 10^{-10} mbar was maintained by an ion-getter pump and a closed-cycle cryopump. The cesium flux to the experimental region was controlled by means of a gate valve. At these conditions it was possible to observe a single trapped atom for as long as 10 min.

Fluorescence of the atoms trapped in the MOT was observed with avalanche photodiodes (APD, EG&G) in single photon counting mode with measured photon detection efficiency of 50% at the wavelength $\lambda = 852$ nm. A lens mounted inside the vacuum chamber collected the fluorescence light from a solid angle of 4.5% (Fig. 1). The figure does not show an aperture system around the MOT inside the vacuum chamber for trapping most of the stray laser light. After passing through a beamsplitter (BS in Fig. 1) and the imaging optics the light is focused onto the entrance apertures of the APD's. The APD's are cooled to $-10\,^{\circ}$C to reduce their dark count rates below 15 /s. Typical photon counting rates are 3–20 kHz per atom depending on the detuning δ of trapping laser from atomic resonance ($\delta/\Gamma = -8 \ldots -1$, in terms of the natural linewidth $\Gamma = 2\pi \times 5.2$ MHz) and on the laser intensity (typically 15 I_0 per beam in terms of the saturation intensity $I_0 = 1.1\,\mathrm{mW/cm^2}$).

Well separated equidistant steps in the fluorescence signal (Fig. 2) allow us to monitor the instant number of trapped atoms. In Fig. 3 we show an example of photon counting statistics in our experiment. The mean number of photon counts in a given time depends linearly on the atom number N, $\langle n\rangle = \langle n_\mathrm{s}\rangle + N\langle n_\mathrm{a}\rangle$ and shows no dead time effects in the detection system. Here $\langle n_\mathrm{s}\rangle$ and $\langle n_\mathrm{a}\rangle$ are mean photon counts from stray light and one trapped atom, respectively.

There are two contributions to the variance of the number of detected photon counts [8]

$$\langle(\Delta n)^2\rangle = \langle n_\mathrm{s}\rangle + N\langle n_\mathrm{a}\rangle + \langle n_\mathrm{s}\rangle^2 \frac{\langle \Delta I^2\rangle}{\langle I\rangle^2} + N^2\langle n_\mathrm{a}\rangle^2 \frac{\langle \Delta R^2\rangle}{\langle R\rangle^2}\,. \tag{1}$$

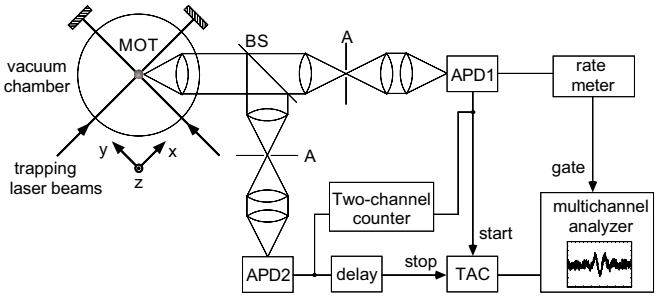

Fig. 1. Experimental setup for photon correlation measurements (see text for details). In the image planes of both telescopes 150 μm pinholes (A) are placed for spatial filtering of the stray light. The z-axis is the symmetry axis of the magnetic quadrupole filed

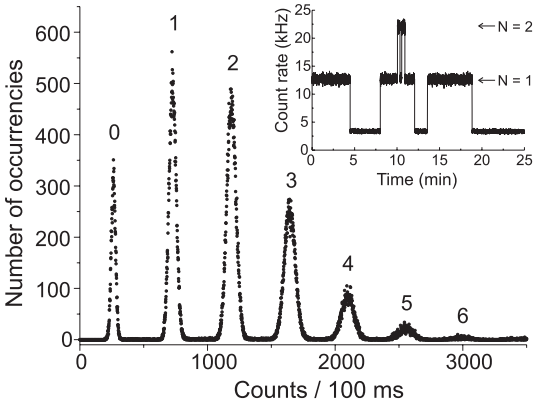

Fig. 2. Distribution of fluorescence count rates (a three hour data run) consists of peaks corresponding to $N = 0, 1, 2 \ldots$ atoms. Inset: typical MOT fluorescence signal detected with an APD at laser detuning $\delta = -12$ MHz. Well separated discrete fluorescence levels correspond to empty trap (stray light from the trapping lasers), one, and two atoms, respectively

The first two terms are equal to the mean number of photon counts and thus they describe the shot-noise contribution (dotted line in Fig. 3). The last two terms are induced by fluctuations of the trapping laser intensity (classical wave noise). The effect of laser intensity fluctuations on the fluctuations of the scattering rate R is partially suppressed due to saturation

$$\langle \Delta R^2\rangle/\langle R\rangle^2 = \left[\frac{1+(2\delta/\Gamma)^2}{1+(2\delta/\Gamma)^2+s_0}\right]^2 \langle \Delta I^2\rangle/\langle I\rangle^2 \tag{2}$$

by a factor about 0.2 in this case. The solid line in Fig. 3 presents the expected variance calculated from measured parameters (laser detuning $\delta = -4\Gamma$, saturation parameter $s_0 = 80$ and residual laser intensity fluctuation $\sqrt{\langle \Delta I^2\rangle}/\langle I\rangle = 1.3\%$). The value measured for a single trapped atom deviates from the expectation by no more than 4%. A still more precise and comprehensive analysis can be obtain from photon correlation measurements.

At the time scales of Figs. 2 and 3 we observe no correlations in the resonance fluorescence and the measurement is essentially shot-noise limited. Dynamical atomic processes induce deviations from the Poissonian photon statistics

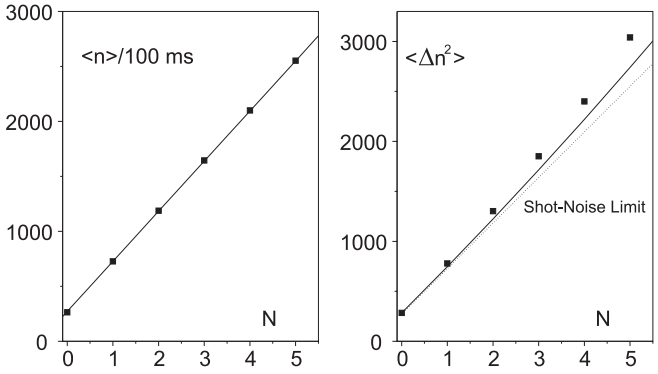

Fig. 3. Photon count statistics corresponding to the data run of Fig. 2. *Left*: The mean photon counts $\langle n\rangle$ vs. the trapped atom number N. The linearity in the peak separation is obeyed to better than 2%. *Right*: Widths $\langle \Delta n^2\rangle$ of the peaks in Fig. 2 slightly exceed the shot-noise limit due to residual intensity fluctuations of the trapping laser beams (see explanations in text)

($g^{(2)}(\tau) = 1$) at shorter time scales, however, and can be analyzed by photon correlation measurements.

We use two methods to record two-photon correlations. At short time scales below 20 μs a Hanbury Brown and Twiss type set-up [9] with a beamsplitter and two photodetectors is used (Fig. 1). After pulse shaping and amplification the pulses from both photodiodes are directed to the start and stop inputs of a time-to-amplitude converter (TAC) and a multichannel analyzer. An artificial delay in the stop-pulse line translates the time origin of the TAC to the 250-ns channel. This single-stop technique has high time resolution better than 1 ns and provides the waiting time distribution which is proportional to the intensity correlation function if the coincidence probability within the relevant time span τ is much smaller than 1. At higher count rates (or for larger time scales) a systematic error is introduced [10] since only the first detected stop-photon is used for timing purposes and any subsequent stop-photons are lost. Thus, even for constant correlation functions the probability to detect a coincidence at delay τ decays as $\exp(-\tau/\tau_0)$ with counting rate τ_0^{-1}. This problem is eliminated by recording arrival times of all photons (with the two-channel counter in Fig. 1) at time scales > 100 ns, which are then correlated by a computer program. Such a multiple-stop technique does not need any corrections at longer times, agrees perfectly with the single-stop results at shorter times, and allows quantative analysis of the correlation signal amplitude. In addition we have monitored the counting rate of one of the photodiodes to control the number of trapped atoms with time resolution 100 ms.

2 Intensity correlations

The only information source accessible for a non-invasive study of laser-cooled atoms is the fluorescence light emitted by the atoms. One method is to combine this fluorescence with a strong local-oscillator laser beam on a photodiode and to detect the spectrum of the beat signal [11–13]. This optical heterodyne technique was used to show atom localization and quantized atomic motion in standing-wave optical potentials [12]. In a related method one observes *temporal* fluctuations in the fluorescence intensity caused by beating of the Doppler shifted light from different atoms. This idea was used to study atomic transport in a standing-wave laser field at the scale of the optical wavelength [14] and for spectral analysis of scattered light from atoms in optical molasses [15] by analyzing intensity correlations.

Another application of the intensity correlation technique is the demonstration of non-classical behavior in resonance fluorescence, e.g. photon antibunching [16–18]. In such experiments intensity fluctuations are caused by the single atom time dependence of excitation in the light field (Rabi oscillations). The presence of several atoms or, even worse, fluctuations of the atom number in the observation region leads to smearing out of the correlation signal. This makes a single trapped ion or atom the best experimental choice [18].

The intensity correlation function (or equivalently second order degree of coherence) [19] defined classically in terms of the fluorescence intensity $I(t)$ is given by

$$g^{(2)}(\tau) = \frac{\langle I(t)\, I(t+\tau)\rangle}{\langle I(t)\rangle^2}\ , \tag{3}$$

where the angle brackets denote averaging over time t. For any real light source correlations always vanish at very long delays $\tau \to \infty$ and hence we have $\langle I(t)\, I(t+\tau)\rangle \to \langle I(t)\rangle\langle I(t)\rangle$ and $g^{(2)}(\tau) \to 1$. At time scales τ of characteristic intensity fluctuations $g^{(2)}(\tau)$ shows deviations from unity. It is thus often convenient to present and discuss the physical information in the form $g^{(2)}(\tau) - 1$. We also define $g^{(2)}(0) - 1$ as *visibility* V which is identical to the normalized variance of the intensity,

$$V = g^{(2)}(0) - 1 = \frac{\langle I(t)^2\rangle - \langle I(t)\rangle^2}{\langle I(t)\rangle^2} = \frac{\langle \Delta I^2(t)\rangle}{\langle I(t)\rangle^2} \geq 0\ . \tag{4}$$

In the photon language $g^2(\tau)$ describes the conditional probability of detecting a second photon at time τ after a first one was detected at $t = 0$ [20].

The physical information contained in $g^{(2)}$ is the experimental and theoretical quantity of prime interest. For a single light-field mode the correlation function $g_N^{(2)}$ from N atoms is connected to the single-atom $g^{(2)}$ by [19]

$$g_N^{(2)}(\tau) = \frac{1}{N}\left[g^{(2)}(\tau) + (N-1)\left(1 + |g^{(1)}(\tau)|^2\right)\right]\ . \tag{5}$$

In the limit of a large number of atoms, $N \gg 1$, (5) reduces to $g^{(2)}(\tau) = 1 + |g^{(1)}(\tau)|^2$. In this case the intensity correlation function is simply related to the *field* correlation function $g^{(1)}(\tau)$ describing interference between light fields from different atoms [14, 15]. The first-order coherence $g^{(1)}(\tau)$ is the Fourier transform of the frequency spectrum produced by the sample. The information contained in $g^{(2)}(\tau)$ in this case is also available by other methods for example by optical heterodyne techniques [11, 12].

In contrast, in few-atom experiments fluorescence is usually collected from a large solid angle. As a result many Fresnel (coherence) zones are observed and interference effects of light fields from different atoms are canceled. The *intensity* correlations survive due to their insensitivity to the field phase. Thus the photon coincidence number from N atoms detected in channel τ is proportional to

$$Ng^{(2)}(\tau) + N(N-1)\ , \tag{6}$$

with a transparent meaning: the probability of detecting a coincidence (two photons) from one and the same atom is proportional to N and their eventual correlation is described by $g^{(2)}(\tau)$. Additionally one has occasional coincidences of two uncorrelated photons from two different atoms. The signal (6) is not sensitive to inhomogeneous broadening and displays individual atom effects only ($g^{(2)}(\tau)$ in its pure form).

3 Internal dynamics

One of the best ways to study internal dynamics of an atom is to measure the two-photon correlation function $g^{(2)}(\tau)$ of the light emitted by the atom. Let us consider for simplicity a single two-level atom interacting with a near resonant laser beam. The state of an excited atom evolves continuously in the absence of a measurement, but theory predicts a sudden jump to the ground state when a photon is detected. This measurement 'triggers' the atom to the initial conditions

$\rho_{11}(0) = 1$ and $\rho_{22}(0) = 0$, where $\rho_{11}(t)$ and $\rho_{22}(t)$ are the density matrix elements representing the population of the ground and excited atomic state, respectively. The normalized probability for detecting a second spontaneously emitted photon is now proportional to the population of the excited atomic state ρ_{22} according to [19]

$$g^{(2)}(\tau) = \rho_{22}(\tau)/\rho_{22}(\infty)\,. \tag{7}$$

Thus, a measurement of $g^{(2)}(\tau)$ gives direct access to the internal dynamics of the atom (at ns time scale in our case).

For a single atom $g^{(2)}(\tau)$ vanishes identically for $\tau = 0$ which is a reflection of the fact that the atom cannot emit two photons simultaneously. This phenomenon is called 'photon antibunching' and has attracted much interest in the past [16–18] since it is regarded as an important manifestation of the quantum nature of light. All classical fields have autocorrelations $g^{(2)}(0) \geq g^{(2)}(\tau)$, and a value $g^{(2)}(0) - 1 < 0$ is indeed a signature for a pure quantum effect. Photon antibunching has been observed from atoms in a dilute atomic beam [16] and [17], from atomic ions in a Paul trap [18] and also from single molecules on a solid surface [21].

If the coupling strength between atomic transition and the exciting light is large enough, transient oscillations in the population of the excited state corresponding to excitation and deexcitation cycles can be seen for $\tau > 0$ (Rabi oscillations). For τ larger than the life time of the excited state the correlations die out due to the fluctuations of the vacuum field.

The two-photon correlations in the fluorescence of trapped neutral atoms measured separately for different atom numbers are shown in Fig. 4. Photon antibunching and distinctive Rabi oscillations are clearly seen. Note that the correlations do not show transition to photon bunching (maximum at $\tau = 0$) with increasing N. It is much easier to observe the pure quantum-mechanical effect of photon antibunching in the fluorescence light from two (or few) atoms than bunching, whose classical interpretation, as a result of intensity fluctuations, is straightforward [22].

The Rabi frequency is a measure of the interaction strength between the atom and the light field and contains information on the local field polarization and the instant internal state of the atom. During the measurement the Rabi oscillations are averaged over atomic trajectory through the trap. Although the light in the three-dimensional interference pattern has all kinds of polarizations at different places in the MOT, and in spite of the complicated multilevel structure of the cesium atom [23] the Fourier transform of $g^{(2)}(\tau)$ (corrected for the exponential decay) shows only one significant component. Therefore we have tried to understand the measurements with a simple model: a two-level atom driven by near resonant laser radiation, whose correlation function $g^{(2)}(\tau)$ for resonance fluorescence is given in [24]. The parameters for the two-level atom were taken from the transition between the outer Zeeman sublevels in the ground $6S_{1/2}F = 4, |m_F| = 4$ and excited $6P_{3/2}F' = 5, |m_{F'}| = 5$ states of cesium. The measured dependence of the Rabi frequency on the laser detuning δ follows $\Omega^2 = \Omega_R^2 + \delta^2 - (\Gamma/4)^2$, Ω_R being the Rabi frequency at resonance. Its absolute value $\Omega_R/2\pi = 31.1 \pm 0.2$ MHz agrees within 6% with the value determined from power broadening of the spectral line. It also corresponds to 6 times the estimated intensity of one laser beam.

This simple model reproduces the observed oscillations surprisingly well (solid line in Fig. 4). The observation suggests that due to optical pumping a trapped atom spends most of its time in the state that interacts most strongly with the local field and is forced to behave, to a good approximation, like a two-level system.

The measured correlations at ns time scale lie slightly above the theoretical curves indicating additional intensity correlations induced by atomic motion through the trap at larger time scales. Polarization-resolved analysis of intensity fluctuations will shed additional light on this observation.

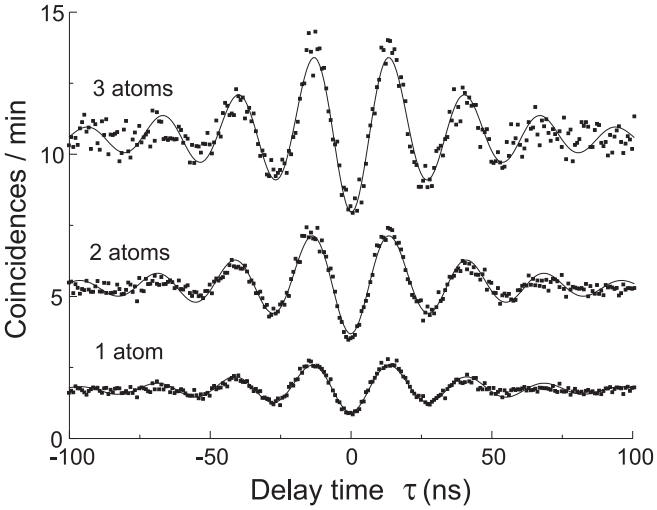

Fig. 4. Two-photon correlation in the resonance fluorescence from N atoms trapped in the MOT. The amplitude $g^{(2)}(0)$ scales as $1/N$ according to (6). The *solid line* is a fit with only one fit parameter, the Rabi frequency, (all count rates were measured independently) for laser detuning $\delta = -20$ MHz and natural linewidth $\Gamma/2\pi = 5.2$ MHz. The integration times were 236, 247 and 69 min for $N = 1, 2$ and 3, respectively

4 Global transport: position correlations

The fluorescent radiation does not show any correlations at time scales beyond some milliseconds. We have, however, generated a fluorescence signal depending on atomic position by introducing a sharp edge into an intermediate trap image (points A in Fig. 1) and analyzed the fluctuations of fluorescence intensity which is now partially obstructed.

This positionally encoded intensity correlation depends on the transport properties of the atom at macroscopic ($> \lambda$) length scales. Since the uncertainty in the atom position due to diffraction in the imaging system is more than an order of magnitude smaller than the trap size, we assume for simplicity that a trapped atom can be seen only if it stays at $z > z_1$, where z_1 is the upper edge position. Registration of a photon then locates the atom in the unobstructed part of the trap volume, and in the absence of stray light the function $P_>(\tau) = \langle I(t)I(t+\tau)\rangle / \langle I^2(t)\rangle$ describes the conditional probability of seeing the atom at time $t = \tau$ after it has been seen at $t = 0$. Here $I(t)$ is the detected intensity of the atom fluorescence. Including the reduction of contrast by the averaged detected stray-light intensity $\langle S\rangle$ we find for the intensity

correlation

$$g^{(2)}(\tau) = 1 + \frac{P_>(\tau)/P_>(\infty) - 1}{(1 + \langle S\rangle/\langle I\rangle)^2} \,. \tag{8}$$

Note that for zero stray light, $\langle S\rangle = 0$, one obtains $g^{(2)}(\tau) = P_>(\tau)/P_>(\infty)$ for this classical correlation in close analogy to the quantum two-level system (7). By numerical simulations we have also checked that geometric aberrations of the imaging system further reduce the contrast but do not change the form of the correlation function.

The long-range trapping force in the MOT arises from unbalanced radiation pressure due to the Zeeman detuning in the magnetic quadrupole field. The radiation force in the MOT averaged over several scattering cycles (in time) and over several wavelengths (in space) can be expressed as a damped harmonic force with spring constant κ and friction parameter α. In a simple model and at temperature T (which has the meaning of an average kinetic energy of the trapped atom) random fluctuations of the friction force may be characterized by a diffusion constant $D = kT/\alpha$. Treating the MOT as an effective harmonic potential charaterized by a spring constant κ and by a friction coefficient α we may use the theory of Brownian motion [25] to derive a Fokker–Planck equation for atomic motion in the MOT,

$$\frac{\partial}{\partial t} f = \frac{\kappa}{\alpha}\frac{\partial}{\partial z}(z f) + \frac{kT}{\alpha}\frac{\partial^2}{\partial z^2} f \,. \tag{9}$$

Here the function $f = f(z, z_0, t)$ describes the probability density for the atom to be at time t at z for the initial atom position $z(0) = z_0$ and has the form

$$f(\hat{z}, \hat{z}_0, t) = \frac{1}{a(t)\sqrt{\pi}} \exp\left[-(\hat{z} - \hat{z}_0 \mathrm{e}^{-\beta t})^2/a^2(t)\right] \,, \tag{10}$$

which evolves into the steady state probability distribution for large times $f(\hat{z}, \hat{z}_0, \infty) = \exp(-\hat{z}^2)/\sqrt{\pi}$. Here we have introduced for convenience $\hat{z} = z\sqrt{\kappa/2k_\mathrm{B}T}$, $a^2(t) = 1 - \exp(-2\beta t)$ and $\beta = \kappa/\alpha$.

For the simplest case of a symmetrical edge position $z_1 = 0$ with respect to the trap volume the correlation function can be given analytically,

$$g^{(2)}(\tau) = 1 + \frac{2}{\pi}\frac{\arccos\sqrt{[1 + \exp(-\beta\tau)]/2}}{(1 + \langle S\rangle/\langle I\rangle)^2} \,. \tag{11}$$

The positional correlations measured at different laser detunings are shown in Fig. 5. From a fit according to (11) we find position damping times β^{-1} in good agreement with data of [26] (inset in Fig. 5). In those experiments the position damping time was measured by monitoring the motion of the trap center as a function of time after having introduced a small displacement using an additional magnetic field. Several precautions had to be taken to ensure that the situation does not deviate significantly from the steady-state dynamics, implying several restrictions on experimental parameters. In contrast, our method is a non-invasive one and every measurement in Fig. 5 has been carried out in no longer than 4 min.

We note that we have also succeeded in splitting the secondary image and monitoring the upper and lower half with two separate photon counters acting as a crude two pixel camera. Combining these two correlations effectively reduces the stray light contribution to the measurements. It is clear that with more sophisticated camera equipment the motion of a single atom in a trap can be monitored directly [27].

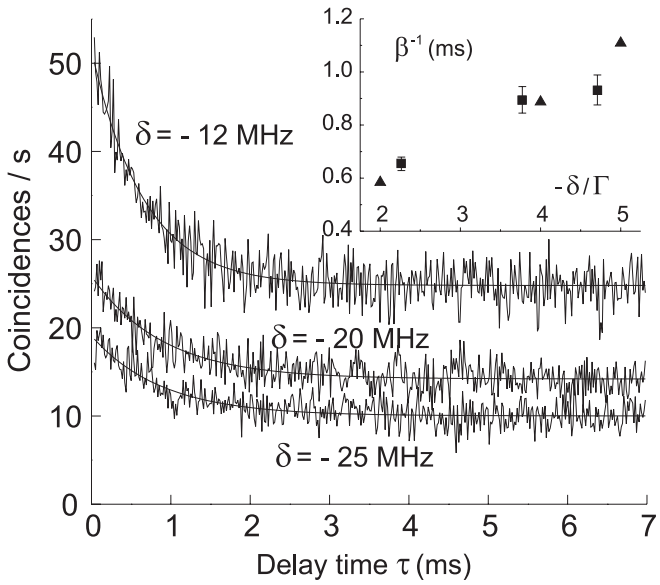

Fig. 5. Intensity autocorrelations recorded from the half image of the trap at different laser detunings δ. The data are divided by the integration time which was about 4 min for all measurements. *Solid lines* are fits according to (11). Inset: Position damping times $\beta^{-1} = \alpha/\kappa$ as a function of laser detuning δ: □ – our data, △ - from Fig. 17 of Ref. [26] multiplied by 5.2/375, the ratio of the magnetic field gradients used in the two experiments

5 Microscopic transport: polarization correlations

Moving through the trap the atom visits various spots of the light interference pattern with different intensity and polarization [28]. The polarization of resonance fluorescence is determined by the magnetic orientation of the atom which in turn depends on the local light field [29] and changes on the time scale of atomic transport over an optical wavelength λ. Thus, in addition to correlations of the total intensity (3) one also expects polarization effects, that is the correlation $g^{(2)}_{\alpha\beta} = \langle I_\alpha(t) I_\beta(t+\tau)\rangle / \langle I_\alpha(t)\rangle\langle I_\beta(t)\rangle$ measured between any polarization components α and β which should strongly depend on the atomic motion and the light-field topography.

5.1 Experimental results

Photon correlations measured between various polarization components of single-atom fluorescence are presented in Fig. 6. We have observed auto ($\sigma^+\sigma^+$) and cross ($\sigma^+\sigma^-$) correlations with surprisingly large visibility for circular components, but no correlations for linear polarizations, see inset in Fig. 6. Qualitative agreement of the experimental data and expectations is found for the order of magnitude of the time constant. For a Cs atom at the Doppler-limit temperature (125 μK) it takes a time $\lambda/v \approx 2\pi 30/\Gamma$ to pass a distance λ. It gives for the decay time of the correlation function a value of $(kv)^{-1} \approx 1\,\mu\mathrm{s}$. Preliminary results indicate that the decay time increases with decreasing

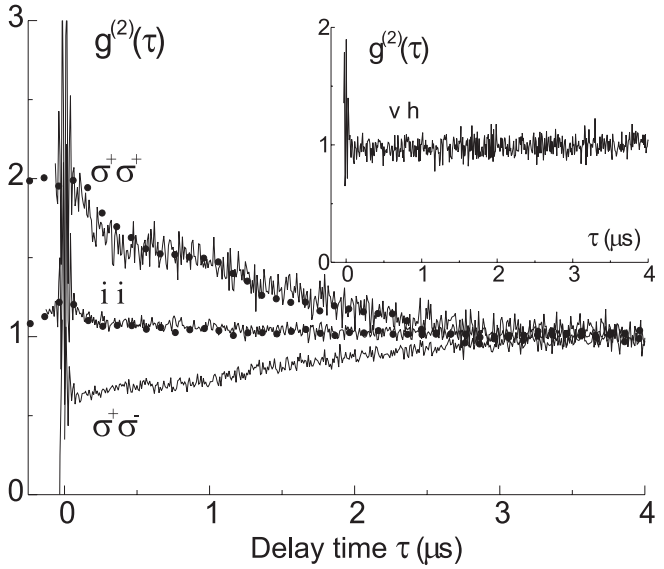

Fig. 6. Polarization correlations of a single atom fluorescence at trapping laser detuning $\delta = -20$ MHz. *Solid lines*: single-stop measurements corrected for exponential decay, showing at very short time scales the Rabi oscillation phenomenon described above; *dots*: multiple-stop measurements with time resolution of 100 ns. Polarization v is defined to be parallel to the trap symmetry axis z, h is orthogonal to both z and the observation direction xy (see Fig. 1)

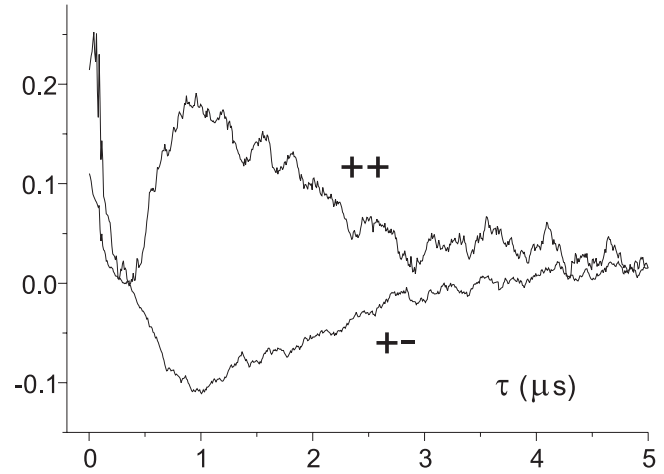

Fig. 7. Residuals of the auto (++) and cross (+−) correlation functions $g^{(2)}_{+\pm}(\tau) - 1$ in Fig. 6 after substraction of a pure exponential decay $\pm\exp(-\tau/\tau_0)$ with $\tau_0 = 1.2\,\mu$s. Note that similar bunching-like contributions occur in both correlation functions at the time scale of the decay time constant (about 0.4 μs) of the total fluorescence intensity correlation function (ii in Fig. 6)

laser intensity as one would expect. Furthermore, in contrast to photon correlation measurements with many laser-cooled atoms reported in [14] we find auto $g^{(2)}_{++}(\tau)$ and cross $g^{(2)}_{+-}(\tau)$ correlation functions having the same time constants (Fig. 7). We have tested the sum rule for circular component correlations $g^{(2)}_{++}(\tau) + g^{(2)}_{+-}(\tau) = 2g^{(2)}(\tau)$ [30] by measuring all correlation functions independently and found a good agreement. The total intensity correlations $g^{(2)}(\tau)$ at μs time scale explain slight deviations of measured photon correlations from the two-level model at ns time scale. However, the correlations for circular polarization are much stronger ($g^{(2)}_{++}(0) \simeq 2$) than predicted according to a simple model (see below). Furthermore, they exhibit reproducible deviations from the pure exponential decay.

5.2 A simple 1D model

Because of the entanglement of internal and external degrees of freedom, a proper description of the atomic dynamics is a non-trivial problem even in a one-dimensional standing light field and for a simple transition $J = 1/2 \rightarrow J' = 3/2$ [31, 32]. We do not intend here to present a sophisticated theory but rather to describe the atomic motion in a simple phenomenological way and to look at different characteristic situations and their effect on the correlation function.

In order to gain physical insight let us start with an atom modeled by a classical emitter ($J = 0 \rightarrow J = 1$ transition) with an induced dipole moment proportional to the local light field. If we describe the position dependent fluorescence intensity of polarization component α by $I_\alpha(z)$, and the probability density for the atom at time t to be at z if its initial position was $z(0) = z_0$ by $f(z, z_0, t)$, then the corresponding correlation function is given by

$$g^{(2)}_{\alpha\beta}(\tau) = \iint_{-\infty}^{\infty} \mathrm{d}z\,\mathrm{d}z_0 I_\alpha(z_0) I_\beta(z)\, f(z_0, z_0, \infty) \times f(z, z_0, \tau)/\langle I_\alpha(t)\rangle\langle I_\beta(t)\rangle\,. \tag{12}$$

We consider now three characteristic one-dimensional light field configurations, produced by two plane waves counterpropagating along z with the same frequency, equal amplitudes and polarizations ε and ε' [33, 34]:

– $\sigma^+\sigma^-$ case ('one-dimensional MOT'): A pair of two circularly polarized laser beams with the same handedness ($\varepsilon = \hat{\boldsymbol{e}}_+ = -(\hat{\boldsymbol{x}} + \mathrm{i}\hat{\boldsymbol{y}})/\sqrt{2}$) and ($\varepsilon' = \hat{\boldsymbol{e}}_- = (\hat{\boldsymbol{x}} - \mathrm{i}\hat{\boldsymbol{y}})/\sqrt{2}$) produces a local polarization that is linear everywhere with a direction of polarization that rotates a full turn every wavelength [35]

$$\boldsymbol{E} \propto (\sin kz)\hat{\boldsymbol{x}} + (\cos kz)\hat{\boldsymbol{y}}\,. \tag{13}$$

– In the lin ⊥ lin optical lattice, produced by two counterpropagating plane waves with orthogonal linear polarizations ($\varepsilon = \hat{\boldsymbol{x}}$ and $\varepsilon' = \hat{\boldsymbol{y}}$), the total electric field can be decomposed into two standing waves of σ^+ and σ^- polarization, offset by $\lambda/4$ so that the antinodes of one coincide with the nodes of the other [35]

$$\boldsymbol{E} \propto \mathrm{i}(\sin kz)\hat{\boldsymbol{e}}_+ + (\cos kz)\hat{\boldsymbol{e}}_-\,. \tag{14}$$

– The textbook standing wave (*lin* || *lin* case) comprising two counterpropagating plane waves with equal linear polarization ($\varepsilon = \varepsilon' = (\hat{\boldsymbol{x}} + \hat{\boldsymbol{y}})/\sqrt{2}$), has a total electric field of the form [35]

$$\boldsymbol{E} \propto (\sin kz)(\hat{\boldsymbol{x}} + \hat{\boldsymbol{y}})\,. \tag{15}$$

The two first cases have constant light intensity $I \propto |E|^2$ everywhere and show polarization gradients (of corkscrew and Sisyphus type [33]), while in the third case one has pure

Table 1. Positionally dependent polarization components in different 1D light field configurations along with corresponding intensity correlation functions. z is the atom position and k is the wave number. The intensity I_x (I_y) radiated in the z-direction is measured after passing through a polarizing filter oriented along x (y). I_+ (I_-) is measured after passing through a $\lambda/4$-plate oriented at 45° relative to the x axis and a polarizing filter oriented along x (y)

	$I_x(z)$	$I_+(z)$	$I(z)$	$g^{(2)}_{xx}$	$g^{(2)}_{++}$	$g^{(2)}$	$g^{(2)}_{xy}$	$g^{(2)}_{+-}$
$\sigma^+\sigma^-$	$\propto \sin^2 kz$	const	const	$g^{(2)}_{1D}$	1	1	$2-g^{(2)}_{1D}$	1
lin $\perp$ lin	const	$\propto \sin^2 kz$	const	1	$g^{(2)}_{1D}$	1	1	$2-g^{(2)}_{1D}$
lin $\parallel$ lin	$\propto \sin^2 kz$	$\propto \sin^2 kz$	$\propto \sin^2 kz$	$g^{(2)}_{1D}$	$g^{(2)}_{1D}$	$g^{(2)}_{1D}$	$g^{(2)}_{1D}$	$g^{(2)}_{1D}$

intensity gradients with the same linear polarization everywhere. Combinations of these basic types of 1D standing waves are experienced by an atom on straight-line trajectories in arbitrary 3D monochromatic fields [34]. The fluorescence polarizations in these situations are easy to analyze and are collected in Table 1.

For atomic motion in potential-free space, i.e. for $f(z, z_0, t) = f(z - z_0, t)$ all correlation functions shown in Table 1 have the same form. The diffusion-like probability distribution function of (9) in this case ($\kappa = 0$) has the form $f(z, z_0, t) = \exp\left[-(z-z_0)^2/\xi^2(t)\right]/(\xi(t)\sqrt{\pi})$ and from (12) one easily obtains

$$g^{(2)}_{1D}(\tau) = 1 + \frac{1}{2}\mathrm{e}^{-k^2\xi^2(\tau)} . \tag{16}$$

Here $\xi(t)$ describes the temporal spread of the atomic positional probability. The correlation function contains information on the character of the atomic motion. For instance, diffusion ($\xi^2 \propto t$) is indicated by an exponential decay and ballistic-like motion ($\xi \propto t$) yields a Gaussian decay. All correlations disappear after the atom has travelled a distance of λ. The corresponding decay time constant τ_0 is determined by $\xi(\tau_0)^{-1} = \lambda/2\pi$.

As expected all autocorrelation functions (photon antibunching and Rabi oscillations at ns time scales are neglected here) are 'classical' in nature, i.e. they show 'bunching'. Note also that intensity gradients make equal bunching-like contribution to auto- and cross-correlations of any polarization components (bottom row in Table 1). Using the sum rule for orthogonal polarization components (for example $g^{(2)}_{++}(\tau) + g^{(2)}_{+-}(\tau) = 2g^{(2)}(\tau)$ [30]) one easily sees that in general the visibility of cross-correlation functions cannot exceed the visibility of the corresponding autocorrelations. On the other hand, a cross-correlation measurement can be carried out 4 times faster than the corresponding autocorrelation measurement where only a half of the total fluorescence is detected.

5.3 Extensions of the model

5.3.1 3D light field. The model of a diffusively moving classical emitter can be extended into three dimensions, making any known field configuration analytically accessible, including the magneto-optical trap. With two additional 'polarization screws' for the $\hat{\boldsymbol{x}}$ and $\hat{\boldsymbol{y}}$ directions along with the relative phases ϕ and ψ between these standing waves one obtains for the total electric field in a 3D MOT [36]:

$$\begin{aligned}\boldsymbol{E} &= (\sin kz + \sin ky \cdot \mathrm{e}^{\mathrm{i}\psi})\hat{x} + (\cos kz + \cos kx \cdot \mathrm{e}^{\mathrm{i}\phi})\hat{y} \\ &\quad + (\sin kx \cdot \mathrm{e}^{\mathrm{i}\phi} + \cos ky \cdot \mathrm{e}^{\mathrm{i}\psi})\hat{z}\end{aligned} \tag{17}$$

and for the total light-field intensity

$$\begin{aligned}I &\propto \frac{3}{2} + \cos kx \cos kz \cos\phi + \sin ky \sin kz \cos\psi \\ &\quad + \sin kx \cos ky \cos(\phi - \psi) .\end{aligned} \tag{18}$$

For our observation direction $x - y$ (see Fig. 1) we can now define linear $E_\mathrm{v} = E_z \quad E_\mathrm{h} = (E_x + E_y)/\sqrt{2}$ and circular $E_+ = -(E_\mathrm{v} + \mathrm{i}E_\mathrm{h})/\sqrt{2} \quad E_- = (E_\mathrm{v} - \mathrm{i}E_\mathrm{h})/\sqrt{2}$ polarization components and analytically find correlation functions whose amplitude strongly depends on the relative time phases ϕ and ψ.

In Fig. 8 we show the visibility for a classical emitter moving diffusively in a MOT light field with stable time phases ϕ and $\psi = 0$. As a general rule polarization gradients lead to a bunching (antibunching) contribution to the corresponding auto (cross) polarization correlation while intensity gradients always make equal bunching-like contribution to all correlations. From (18) one can show that maximum intensity gradient is realized for $\phi = n\pi$ and $\psi = m\pi$ (the total intensity is fully modulated with 8 zeros in a λ^3 cube). In this case the polarization of the light field is linear everywhere. With growing ellipticity of the light field ($\phi \to \pi/2$) the intensity gradients decrease while the circular polarization gradients increase.

In the experiment, however, the time phases are not controlled and hence eliminated by averaging, yielding the final

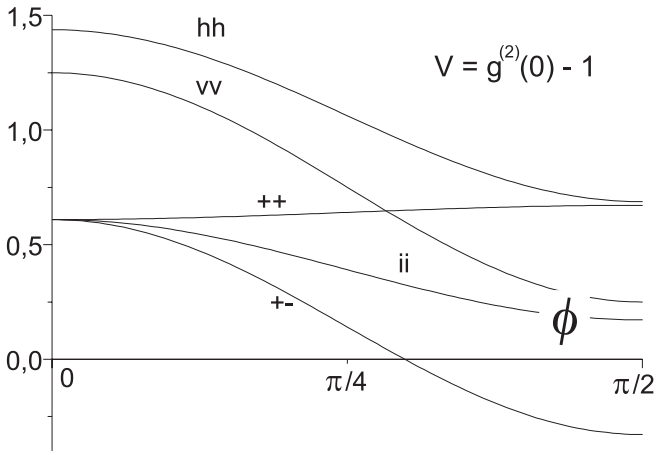

Fig. 8. The correlation function visibility $V = g^{(2)}(0) - 1$ for a classical emitter moving diffusively in a MOT light field as a function of the time phase ϕ ($\psi = 0$). The visibility $V_\mathrm{vh} = -0.125$ is independent of (ϕ, ψ) and is not shown. Due to symmetry of the MOT light field $g^{(2)}_{++}(\tau) = g^{(2)}_{--}(\tau)$. Note also that for $\phi = 0$ (linear polarization everywhere with pure intensity gradients) the auto- and cross-correlations for circular components are equal to the autocorrelation function of the total intensity

Table 2. The coefficients A, B in (19) for total intensity (i), linear (v, h) and circular (+,−) correlation functions along with the visibility $V = g^{(2)}_{\alpha\beta}(0) - 1 = A + B$ for a 3D-MOT light field averaged over time phases ϕ, ψ. Polarization v is parallel to the trap symmetry axis z, h is orthogonal to both z and the observation direction xy (see Fig. 1)

	ii	vh	+−	++
A	0.05	−0.12	0.05	0.05
B	0.28	0	−0.09	0.65
V	0.33	−0.12	−0.04	0.70

result of the form

$$g^{(2)}_{\alpha\beta}(\tau) = 1 + A\mathrm{e}^{-k^2\xi^2(\tau)} + B\mathrm{e}^{-k^2\xi^2(\tau)/2}\,, \qquad (19)$$

where A and B are given in Table 1. The B-term has an effective periodicity $k/\sqrt{2}$ which can be associated with our observation direction along the xy-diagonal of the unit cell.

Due to the contribution of the intensity gradients of the MOT light field to the polarization correlations the general tendency is that the correlations between linear polarizations are more pronounced than for circular: for example the visibility of the cross-correlation function $g^{(2)}_{\mathrm{vh}}$ for linear polarizations should be 3 times larger than the visibility of $g^{(2)}_{+-}$ for circular components (Table 2). This prediction is clearly at odds with the observation. On the other hand, it is obvious that the visibility of the correlation functions in this model is a function of the light-field configuration only, i.e. $g^{(2)}_{\alpha\beta}(0)$ is equal to $\langle I_\alpha(z) I_\beta(z)\rangle / \langle I_\alpha(z)\rangle \langle I(z)_\beta\rangle$ averaged over space.

5.3.2 Multilevel atom. Replacing the classical emitter by a real cesium atom and taking into account optical pumping can shed light on the enhancement of circular component correlations and vanishing visibility for the case of linear polarizations.

1D $\sigma^+\sigma^-$ light field: For a multilevel atom correlations between linear components are less pronounced than for a classical emitter even in a 1D $\sigma^+\sigma^-$ light field which is 'favorable' for observation of linear correlations. A steady-state atom with transition $F = 4 \to F' = 5$ driven by linear polarization spontaneously emits π, σ^+ and σ^- photons (quantization axes parallel to the local light polarization) in proportions 9:4:4. The linear polarization intensity in this case $I_x \propto 4 + 9\sin^2(kz)$ reduces the visibility in (16) by a factor of 3.6.

1D lin ⊥ lin light field: Conversely, the σ^+-intensity (quantization axes parallel to z) in a 1D lin ⊥ lin field as a function of the atom position remains fully modulated, because the atom subjected to $\sigma^+(\sigma^-)$ light can emit only the corresponding circular polarization due to optical pumping. Moreover, due to large angular momentum a Cs atom in an extreme m_F state behaves like a spinning top impeding changes of its magnetic orientation. In Fig. 9 we show the averaged projection of the magnetic moment of Cs atom in a 1D lin ⊥ lin light field calculated from rate equations. Even at places with as much as 30% of the 'wrong' σ^- polarization in the local light field the atom stays mostly in the outermost Zeeman $m_F = +4$ state and coupling with the σ^- component is strongly suppressed by a factor 45 due to difference in the corresponding Clebsch–Gordon coefficients. As a result the spatial dependence of the radiated circular component

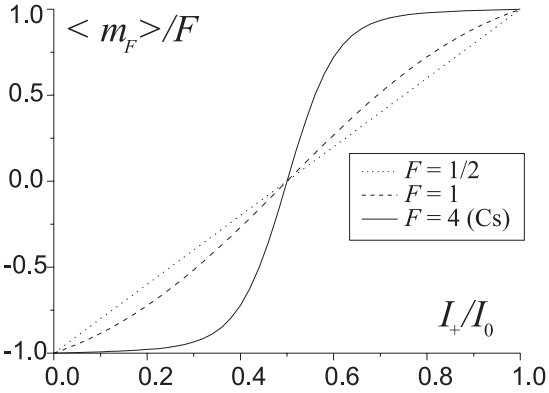

Fig. 9. Averaged magnetic orientation of an atom with transitions $F \to F+1$ in a 1D lin ⊥ lin light field. I_+ is the σ^+-component intensity ($I_+ = I_0 \sin^2(kz)$) of the local light field. The quantization axis is parallel to the light propagation direction z

$I_+(z)$ is a function 'steeper' than $\sin^2(kz)$, which enhances the value of $g^{(2)}_{++}(0)$ to 2.02 instead of 1.5 as for a classical particle.

In the lin ⊥ lin case optical pumping also induces changes in the total intensity: An atom with transition $F = 4 \to F' = 5$ driven by a linear polarized (π) field scatters only about half as many photons to the detector as in the case of circular (σ^+ or σ^-) polarizations. As a result the total scattered intensity is doubly modulated in comparison with circular components explaining the different time constants (approximately a factor of 4) for intensity and polarization correlations, see Fig. 7.

Another reason for the large visibility of circular correlations may be found in the effect of light-induced potentials on atomic transport in the trap. The correlation function amplitude $g^{(2)}_{++}(0)$ for σ^+-polarization component is proportional to $\int \mathrm{d}z I_+^2(z) f(z, z, \infty)$, where $f(z, z, \infty)$ describes the probability of an atom being at z. If the atom prefers places with a certain polarization of the laser field, say σ^+ and σ^-, it will cause stronger fluctuations of the detected $I_+(t)$-signal increasing the value of $g^{(2)}_{++}(0)$ and simultaneously decreasing the visibility of the correlations between the linear components. Thus we believe that $g^{(2)}_{\alpha\beta}(0)$ can be used as a direct measure of the atomic localization in optical potentials. Numerical solution of the Fokker–Planck equation in a periodic potential shows indeed growing visibility of the correlation function $g^{(2)}_{++}(\tau)$ in a 1D lin ⊥ lin light field if the ratio of the potential depth and averaged kinetic energy increases. On the other hand, diffusion is not able to produce any significant deviations from pure exponential decay.

Of course, in the real experiment there are reasons to expect much lower visibility, due to saturation effects or projection onto the observation direction. Thus the measured high visibility of correlations between circular components remains surprising.

6 Conclusion

We have shown that individual-atom trapping allows one to obtain information about atomic internal and external dynamics with excellent contrast, in a non-invasive manner and at all relevant time scales: internal atomic dynamics at nanoseconds, atomic transport and localization at the wavelength

scale at microseconds and atomic movement at larger scales up to the trap size at milliseconds [39].

As a first example we have studied the dynamics of one atom stored in a magneto-optical trap which is by far the most widely used atom trap. In spite of its conceptual simplicity the dynamical behavior of atoms in such a trap is complex due to the large number of degrees of freedom available for an atom and the complicated light field configuration.

Observation of simple Rabi oscillations at the ns scale is surprising in the complicated MOT environment whose interference pattern does not show pure circular polarization at minima of light-induced potentials. Nevertheless, the suggestion that the atom stays the most time in its maximum stretched state is also consistent with the atomic localization in optical potentials indicated by the polarization correlations.

For a quantitative analysis of the polarization correlations in the case of a standard 3D MOT it is desirable not only to have a more sophisticated theoretical model but also to experimentally control the phase relations between the six trapping laser beams. The light field topography strongly depends on these time phases [34] which are not controlled in usual MOT experiments. Expected changes of the temperature and the damping time constant [37] as a function of the relative phases can be explored by applying our method to light configurations with well defined and stable light field topography [38].

It would be also interesting to investigate atom dynamics by observation of single atoms in other systems like optical lattices or polarized samples. The problem of spatial diffusion of atoms in optical lattices remains one of the difficult points in an understanding of laser cooling [31]. Correlation techniques provide, in principle, complete information about the atomic motion encoded in the photon statistics, and spatially resolved photon detection allows one to combine high temporal and spatial resolution. The advantage of single atom observation has been recently demonstrated in [27] where indications for Lévy walks were found by tracing the position of a single ion in a one-dimensional optical lattice.

In the case of a single trapped atom there is no uncertainty in the number of atoms contributing to the signal. The stray-light contribution can be easily distinguished and substracted. Therefore information is obtained not only from temporal properties but also from the amplitude of the correlation signal. For example, a simple comparison of correlations from one and two atoms can reveal any collective motional effects. In the derivation of (6) we have additionally assumed that atoms move independently and therefore also that *intensities* detected from different atoms are uncorrelated, that is $\langle I_i(t) I_j(t+\tau)\rangle = [\delta_{ij}(g_i^{(2)}(\tau)-1)+1]\langle I\rangle^2$. By applying a weak and slowly alternating magnetic offset field we have modeled such a collective motion. Deviations from (6) were seen immediately due to synchronous oscillation of all trapped atoms over our razor blade in the case of motional correlation.

References

1. W. Neuhauser, M. Hohenstatt, P.E. Toschek, H. Dehmelt: Phys. Rev. A **22**, 1137 (1980)
2. Z. Hu, H.J. Kimble: Opt. Lett. **19**, 1888 (1994)
3. F. Ruschewitz, D. Bettermann, J.L. Peng, W. Ertmer: Europhys. Lett. **34**, 651 (1996)
4. D. Haubrich, H. Schadwinkel, F. Strauch, B. Ueberholz, R. Wynands, D. Meschede: Europhys. Lett. **34**, 663 (1996)
5. E.L. Raab, M. Prentiss, A. Cable, S. Chu, D.E. Pritchard: Phys. Rev. Lett. **59**, 2631 (1987); for a recent review see C.G. Townsend, N.H. Edwards, C.J. Cooper, K.P. Zetie, C.J. Foot, A.M. Steane, P. Szriftgiser, H. Perrin, J. Dalibard: Phys. Rev. **A52**, 1423 (1995)
6. A. Höpe, D. Haubrich, G. Müller, W.G. Kaenders, D. Meschede: Europhys. Lett. **22**, 669 (1993)
7. D. Haubrich, A. Höpe, D. Meschede: Opt. Commun. **102**, 225 (1993)
8. L. Mandel, E. Wolf: *Optical coherence and quantum optics* (Cambridge University Press 1995)
9. R. Hanbury Brown, R.Q. Twiss: Nature **177**, 27 (1956)
10. P.B. Coates: J. Sci. Instrum., Ser. 2 **1**, 878 (1968)
11. C.I. Westbrook, R.N. Watts, C.E. Tanner, S.L. Rolston, W.D. Phillips, P.D. Lett: Phys. Rev. Lett. **65**, 33 (1990).
12. P.S. Jessen, C. Gerz, P.D. Lett, W.D. Phillips, S.L. Rolston, R.J. Spreeuw, C.I. Westbrook: Phys. Rev. Lett. **69**, 49 (1992)
13. P. Verkerk, B. Lounis, C. Salomon, C. Cohen-Tannoudji: Phys. Rev. Lett. **68**, 3861 (1992)
14. C. Jurczak, B. Desruelle, K. Sengstock, J.-Y. Courtois, C.I. Westbrook, A. Aspect: Phys. Rev. Lett. **77**, 1727 (1996)
15. S. Bali, D. Hoffmann, J. Siman, T. Walker: Phys. Rev. A **53**, 3469 (1996)
16. H.J. Kimble, M. Dagenais, L. Mandel: Phys. Rev. Lett. **39**, 691 (1977)
17. F.-M. Rateike, G. Leuchs, H. Walther, results cited by J.D. Cresser et al.: In *Dissipative Systems in Quantum Optics*, ed. by R. Bonifatio, Topics in Current Physics, Vol. 27 (Springer, Berlin, Heidelberg 1982) p. 21
18. F. Diedrich, H. Walther: Phys. Rev. Lett. **58**, 203 (1987)
19. R. Loudon: *The quantum theory of light*, 2nd edn. (Oxford University Press, Oxford 1983)
20. For a rigorous quantum-mechanical treatment see R.J. Glauber: Phys. Rev. **130**, 2529 (1963); Phys. Rev. **131**, 2766 (1963)
21. Th. Basché, W.E. Moerner, M. Orrit, H. Talon: Phys. Rev. Lett. **69**, 1516 (1992)
22. In principle, it is possible to observe the transition from photon antibunching to photon bunching even from two atoms by reducing the observation angle aperture. But in our case, due to weak localization of the atoms it would mean a reduction of the count rate far below the dark count rate
23. For measurements of $g^{(2)}(\tau)$ in the case of multilevel ion fluorescence see M. Schubert, I. Siemers, R. Blatt, W. Neuhauser, P. Toschek: Phys. Rev. A **52**, 2994 (1995)
24. H.J. Kimble, L. Mandel: Phys. Rev. A **13**, 2123 (1976)
25. R.K. Pathria: *Statistical Mechanics*, corrected reprint (Pergamon, Oxford 1991)
26. M. Drewsen, Ph. Laurent, A. Nadir, G. Santerelli, A. Clairon, Y. Castin, D. Grison, C. Salomon: Appl. Phys. B **59**, 283 (1994)
27. H. Katori, S. Schlipf, H. Walther: Phys. Rev. Lett. **79**, 2221 (1997)
28. Although the MOT light-field interference pattern strongly depends on the relative time phases between three standing waves, the measured time phase fluctuations are in the acoustic region (below a few kHz). Therefore at μs time scales an atom sees a well defined optical lattice
29. Partial depolarization due to the Hanle effect in the magnetic field is significant only for displacements from the trap center larger than 100 μm and can be neglected here
30. We use $I = I_+ + I_-$ and a reasonable assumption that the statistical properties of orthogonal polarization components are equal $g_{++}^{(2)}(\tau) = g_{--}^{(2)}(\tau)$
31. T.W. Hodapp, C. Gerz, C. Furtlehner, C.I. Westbrook, W.D. Phillips, J. Dalibard: Appl. Phys. B **60**, 135 (1995)
32. S. Marksteiner, K. Ellinger, P. Zoller: Phys. Rev. A **53**, 3409 (1996)
33. J. Dalibard, C. Cohen-Tannoudjii: J. Opt. Soc. Am. B **6**, 2058 (1989)
34. S. Hopkins, A. Durrant: Phys. Rev. A **56**, 4012 (1997)
35. This corresponds to a certain choice for the origin of space and time
36. Note that the *z* corkscrew has a different handedness to the other two because of the quadrupole nature of the MOT magnetic field
37. K. Mølmer: Phys. Rev. A **44**, 5820 (1991); A.M. Steane, M. Chowdhury, C.J. Foot: J. Opt. Soc. Am. B **9**, 2142 (1992); Y. Castin, K. Mølmer: Phys. Rev. Lett. **74**, 3772 (1995)
38. A. Rauschenbeutel, H. Schadwinkel, V. Gomer, D. Meschede: Opt. Commun. **148**, 45 (1998)
39. The dynamics of the trapped atom number (time scale of seconds/minutes) will be discussed elsewhere